Neuron, Volume *91*

Supplemental Information

Oligodendroglial NMDA Receptors Regulate Glucose Import and Axonal Energy Metabolism

Aiman S. Saab, Iva D. Tzvetavona, Andrea Trevisiol, Selva Baltan, Payam Dibaj, Kathrin Kusch, Wiebke Möbius, Bianka Goetze, Hannah M. Jahn, Wenhui Huang, Heinz Steffens, Eike D. Schomburg, Alberto Pérez-Samartín, Fernando Pérez-Cerdá, Davood Bakhtiari, Carlos Matute, Siegrid Löwel, Christian Griesinger, Johannes Hirrlinger, Frank Kirchhoff, and Klaus-Armin Nave

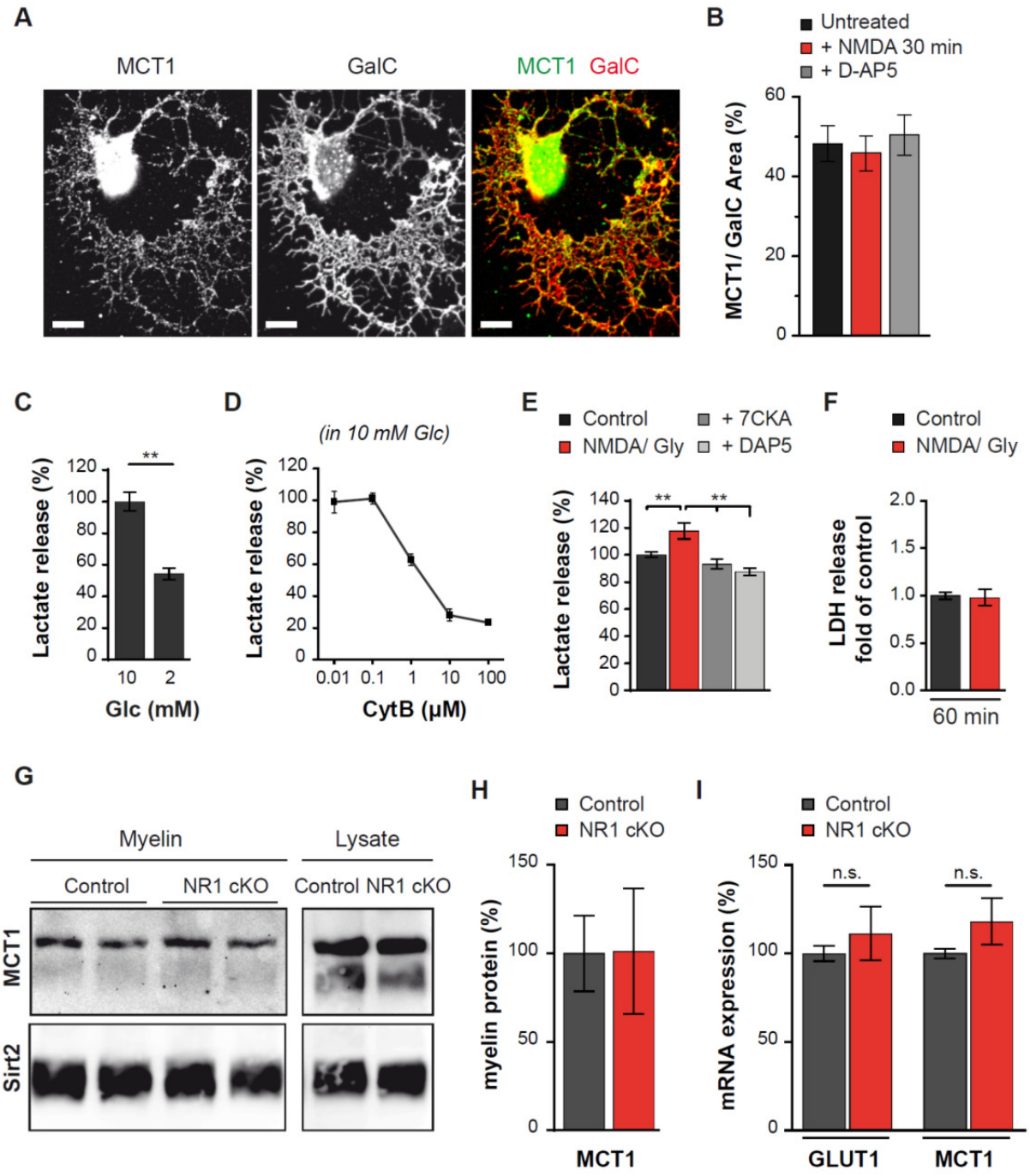

Figure S1 (Related to Figure 1 and 2). Oligodendroglial MCT1 expression is not altered by NMDA receptor stimulation in culture, lactate release from primary oligodendrocytes, and MCT1 abundance in myelin is unchanged in NR1 mutant mice.
A, **B** Immunolabelling of MCT1 in primary oligodendrocytes revealed readily detectable signals at the cell surface. NMDA receptor stimulation for 30 min did not cause any overt MCT1 redistribution, when quantified and normalized to GalC surface staining. Scale bar 10 µm.
C, Lactate release by cultured oligodendrocytes depends on glucose levels in the medium (note K_m for Glut1 is ~ 3 mM).
D, Dose-dependent inhibition by cytochalasin B (CytB), a glucose transporter blocker, reduces lactate release into the medium (containing 10 mM glucose) of oligodendrocytes.
E, Activation of NMDA receptors increases lactate release by 18 % ± 6 % compared to untreated conditions and is specifically blocked by 7CKA or D-AP5 (** $P < 0.01$, n = 5-6; Mann Whitney t test). 7CKA and D-AP5 were used to block the glycinerig and glutamatergic binding site of NMDA receptors, respectively.
F, Measurement of lactate dehydrogenase (LDH), 60 min after the addition of 100 µM NMDA/Gly to the culture medium, yields no evidence for oligodendrocyte death by excitotoxicity.
G, **H**, Western blot analysis of MCT1 in myelin and in total brain lysates from NR1 mutant and control brains. When quantified, MCT1 protein abundance in myelin is not different between NR1 mutants and controls. SIRT2 was used as a loading control
I, mRNA expression of GLUT1 and MCT1 was not significantly altered when comparing samples from enriched white matter of NR1 mutants and littermate controls.

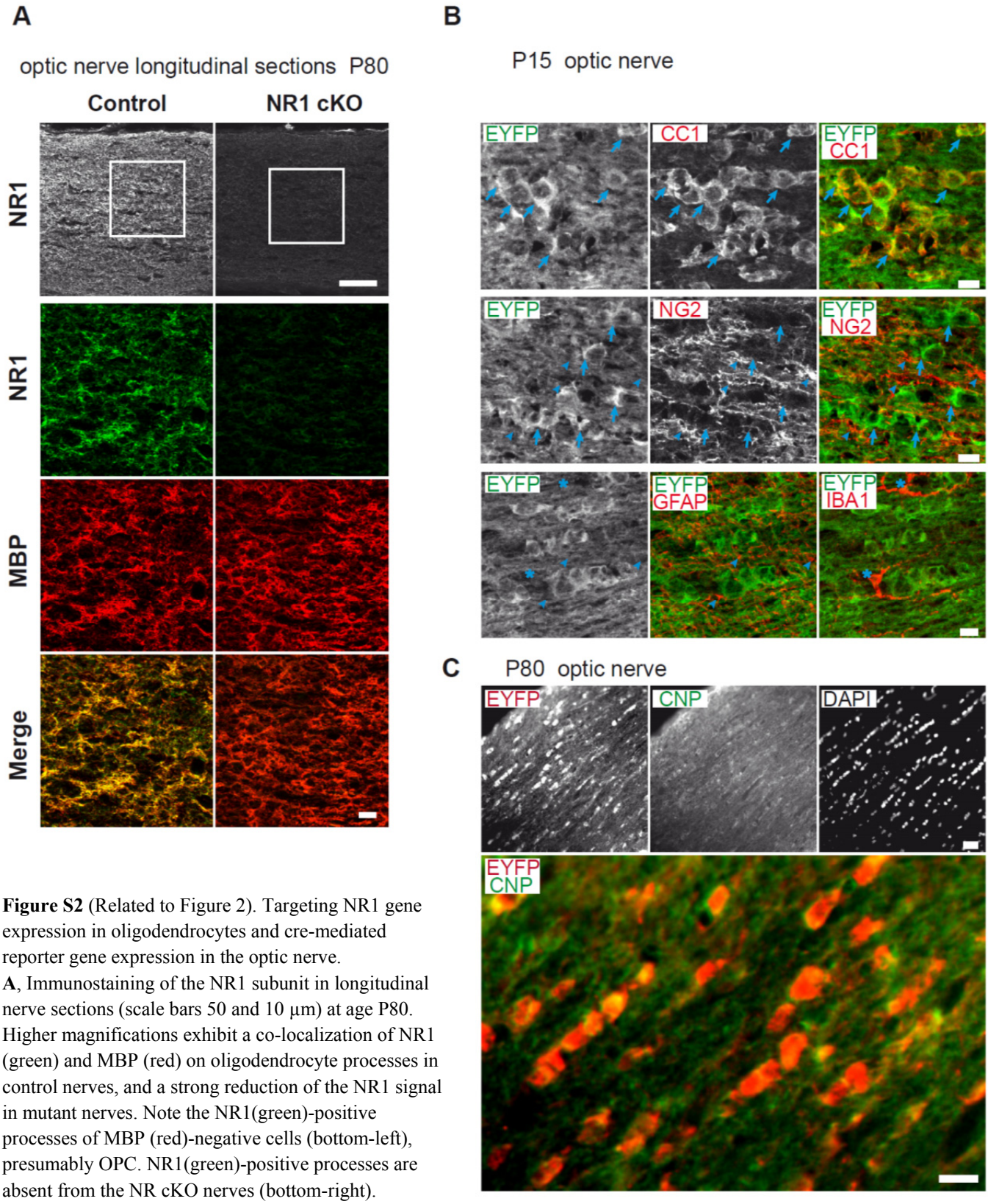

Figure S2 (Related to Figure 2). Targeting NR1 gene expression in oligodendrocytes and cre-mediated reporter gene expression in the optic nerve.

A, Immunostaining of the NR1 subunit in longitudinal nerve sections (scale bars 50 and 10 µm) at age P80. Higher magnifications exhibit a co-localization of NR1 (green) and MBP (red) on oligodendrocyte processes in control nerves, and a strong reduction of the NR1 signal in mutant nerves. Note the NR1(green)-positive processes of MBP (red)-negative cells (bottom-left), presumably OPC. NR1(green)-positive processes are absent from the NR cKO nerves (bottom-right).

B, Cnp1-Cre*ROSA26-floxed-STOP-EYFP mice reveal reporter gene expression in recombined cells of the optic nerve at P15. Confocal sections were immunostained for EYFP (with anti-GFP antibody to enhance reporter signal) and CC1 (mature oligodendrocytes), for EYFP and NG2 (OPCs), and for EYFP, GFAP (astrocytes) and IBA1 (microglia). Arrows indicate mature oligodendrocytes positive for EYFP and CC1. Arrowheads indicate OPC (immunostained for NG2, middle) or astrocytes (immunostained for GFAP, bottom) that are EYFP negative. Asterisks indicate microglia (immunostained for IBA1 but not EYFP). Scale bars 10 µm.

C, Reporter analysis at P80. Epifluorescent overview of longitudinal optic nerve section stained for EYFP and CNP (mature oligodendrocytes). DAPI staining labels nuclei. At higher magnification (bottom) there is a virtually complete overlap of EYFP reporter and CNP expression. Scale bars 20 µm (top), 10 µm (bottom).

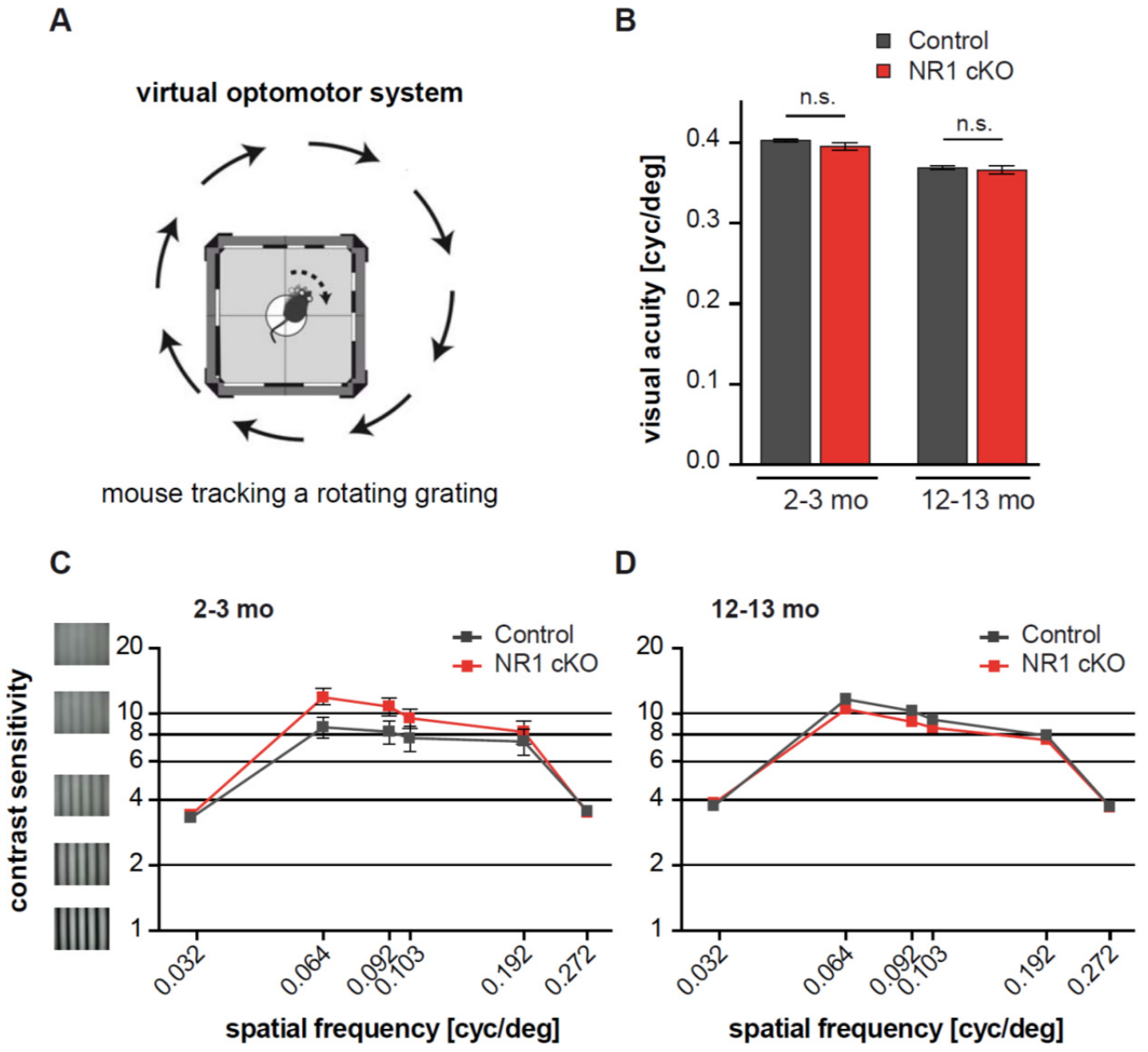

Figure S3 (Related to Figure 3). Behavioural assessment of visual acuity and contrast sensitivity.
A, Visual acuity and contrast sensitivity were measured with a virtual-reality optomotor system. Scheme modified from (Prusky et al., 2004) with permission.
B, Visual acuity was measured with moving gratings of increasing spatial frequency (in cycles per degree = cyc/deg), until the mice stopped tracking. NR1 mutant and littermate controls were examined at 2-3 months and at 12-13 months of age but revealed no difference of performance between genotypes.
C, **D**, Assessment of contrast sensitivity was with stimuli of distinct spatial frequencies that were presented at different contrast levels (1 corresponds to 100 % and 20 to ~ 5 % contrast, see icons (left)). No overt differences were observed between genotypes.

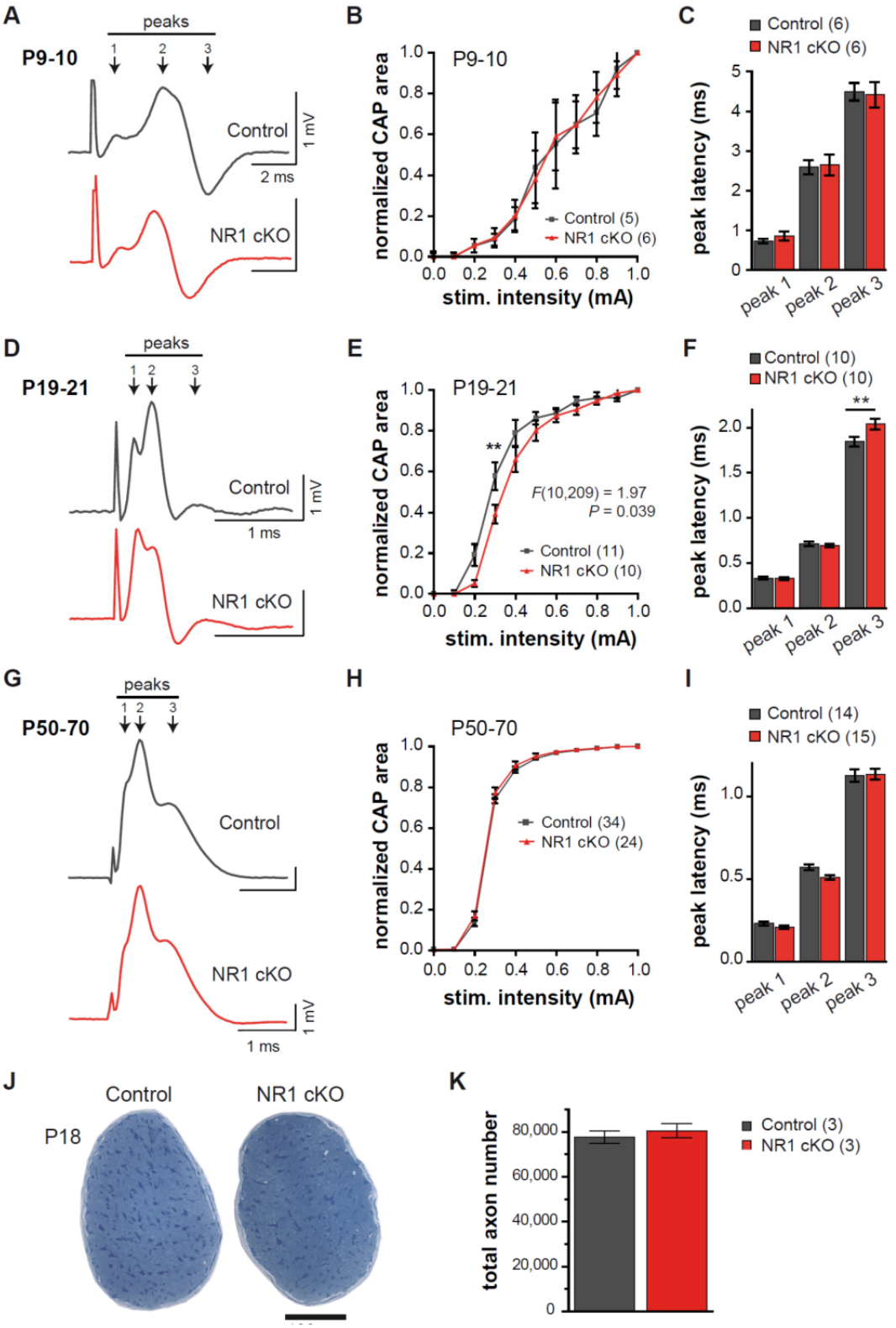

Figure S4 (Related to Figure 3). Optic nerve conduction during postnatal development.
A, **D** and **G**, Representative traces of compound action potentials (CAPs) recorded from acutely isolated optic nerves at three different ages (P9-10, P19-21, and P50-70). Nerves were stimulated with 0.8 mA every 30 s for 15 min. Traces represent CAP averages. **B**, **E** and **H**, Axon excitability of optic nerves measured at different stimulus intensities (0 – 1 mA) in 0.1 mA steps. The CAP area of each stimulus step is normalized to that of maximal stimulation (1 mA).
C, **F** and **I**, Peak latencies of averaged CAPs, recorded at the corresponding ages. **E**, At ages P19-P20, when all optic nerve axons are myelinated, mutant optic nerves displayed a reduction in axon excitability: $F_{interaction}$ (10, 209) = 1.97, P = 0.039, $F_{genotype}$ (1, 209) = 11.71, P = 0.0007, two-way Anova. At stimulus intensities up to 0.3 mA, nerves from controls responded with 58 ± 7 % and nerves from NR1 cKO with 39 ± 5 % of maximal response at 1 mA, ** P < 0.01, two-way Anova, Bonferroni post-test.

F, The conduction delay of peak 3 from NR1 mutants was significantly increased at P19-20 (1.85 ± 0.05 ms vs. 2.04 ± 0.06 ms in control and NR1 cKO, respectively, $P < 0.01$, two-way Anova, Bonferroni posttest). In contrast, in unmyelinated (a – c, P9-10) and in adult, fully myelinated optic nerves (g – i, P50-70) the conduction properties were equal between controls and NR1 mutants.
J, Semi-thin cross sections from epoxy-embedded optic nerves at P18 from control (left) and NR1 cKO (right) mice. No overt difference was observed in nerve cross section area (3 nerves per genotype analysed). Scale bar 100 µm.
K, Total axon number was not altered in NR1 cKO optic nerves (80520 ± 1875) compared to littermate controls (77680 ± 1650, n =3, $P = 0.32$ Student t test). For each optic nerve 400-760 axons from 5-8 randomly taken EM images were counted. Average axon density of each nerve was multiplied with the average total cross section area subtracted from the fraction of non-axonic (glial cell bodies and processes) area.

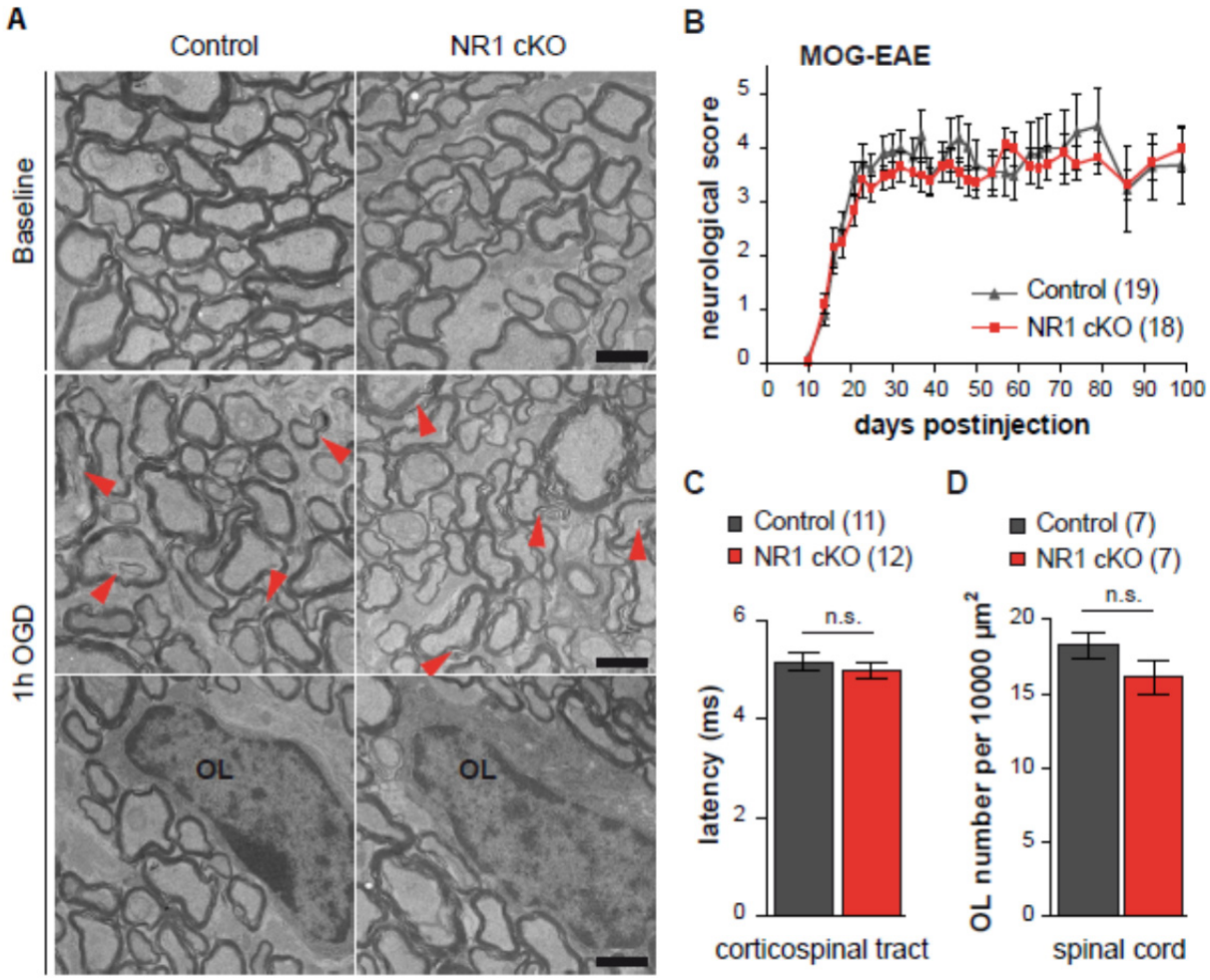

Figure S5 (Related to Figure 4). NR1 mutant white matter tracts are not more vulnerable to injury.
A, Electron microscopic inspection of optic nerves that were subjected to 1 h baseline (upper panel) and 1 h oxygen glucose deprivation (OGD) (middle and lower panel). Ultrastructural damage such as occasional loosening of the myelin sheath (red arrowheads) was identical in both controls and NR1 mutants. In both genotypes there were no morphological signs of oligodendrocyte (OL) death (lower panel). Scale bar 1 µm.
B, Time course of EAE-associated neurological symptoms. Control mice (n=19) and NR1 cKO mice (n=18) were immunized with MOG35-55 peptide and exhibited similar EAE scores, with no difference in the onset of symptoms or severity (see Methods for score).
C, The axon conduction latency in the corticospinal tract of mice with chronic EAE (measured at the end of the EAE experiment) was similar in both groups of animals (control 5.15 ± 0.17 ms (n = 11) vs NR1 cKO 4.98 ± 0.16 ms (n = 12)).
D, At the end of the EAE experiment, the density of oligodendrocytes (CC1+ cells/1,000 µm2) in the spinal cord was not different in NR1 cKO mice (control 18.3 ± 0.9 (n = 7) vs NR1 cKO 16.1 ± 1.2 (n = 7).

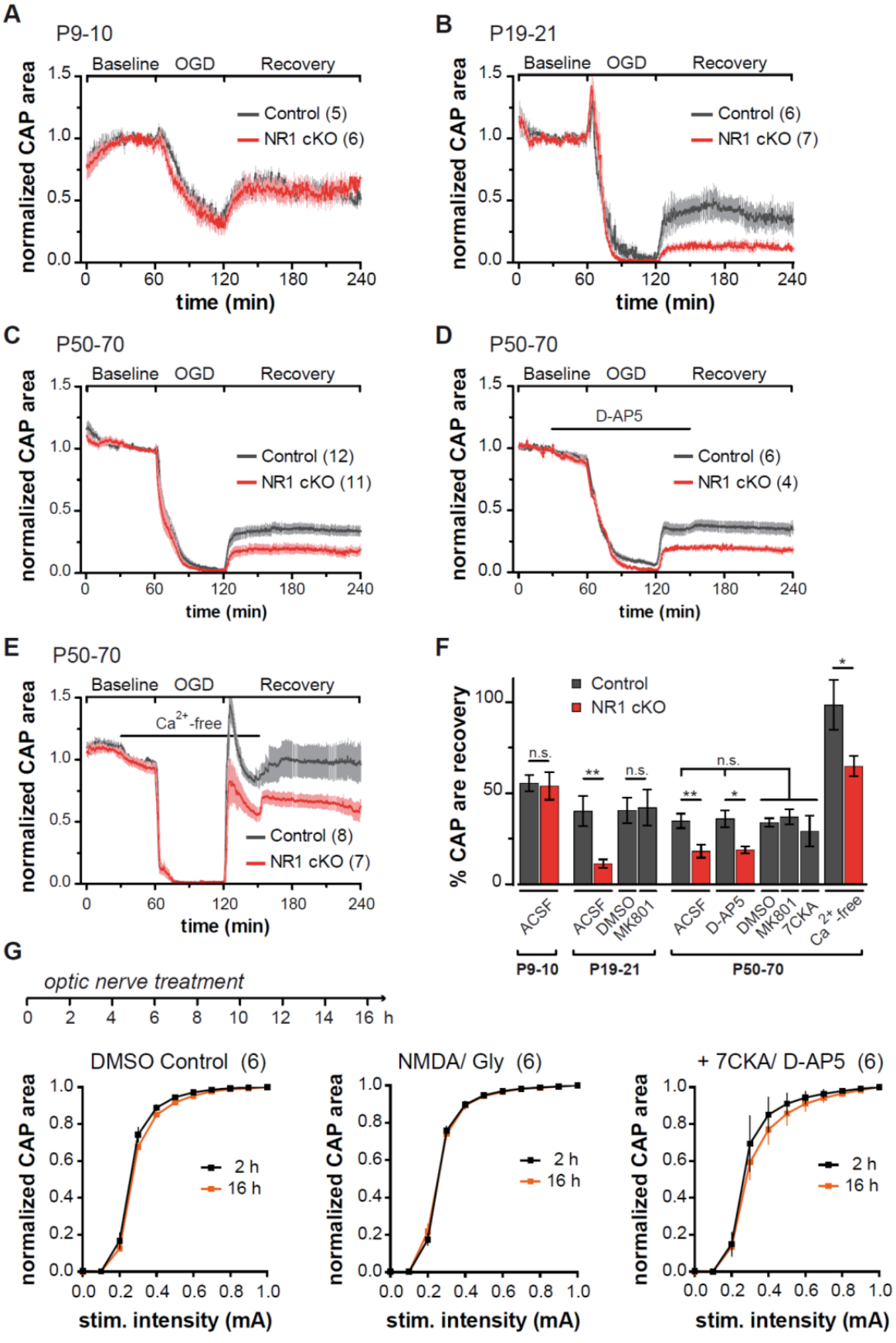

Figure S6 (Related to Figure 4). Recovery of axon function from OGD decreases with myelination and acute NMDA receptor inhibition does not mimic NR1 deficiency

A-E, After 1 h baseline recording (perfused with oxygenated ACSF) optic nerves are subjected to 60 min OGD and then reperfused for a 2 h recovery period with oxygenated ACSF. Functional integrity of axons over time was monitored by quantifying the area under the CAPs (evoked by a supramaximal stimulus) and normalizing to baseline.

A, At P9-10 (when axons are not yet fully myelinated) optic nerves from NR1 cKO showed the same functional decline following OGD and recovery thereafter.

B, At P19-21, myelinated optic nerves from control and NR1 cKO mice exhibited the same rapid loss of conduction, but after OGD nerves from NR1 mutants recovered less well.
C, Following transient OGD optic nerves from adult (fully myelinated) NR1 mutant mice recover less well (-50%) than nerves from littermate controls (same image as in Figure 4A).
D, Incubation of optic nerves from wildtype and NR1 mutants with the NMDA receptor blocker D-AP5 (50 μM, 30 min before OGD onset) did not reveal overt differences of the CAP time course and recovery from OGD when compared to control conditions (ACSF). Note that NR1 mutants recovered -50% when compared to control nerves, suggesting a largely developmental defect.
E, Optic nerves from controls and NR1 mutants were exposed to transient OGD in Ca^{2+}-free conditions (4 mM Mg^{2+} containing 200 μM EGTA). In the absence of free Ca^{2+} axonal recovery is improved in both mutants and controls. Note that axons from NR1 mutants still recovered less well.
F, Comparison of functional axon recovery under different experimental conditions. Wildtype optic nerve axons that were treated with D-AP5, 7CKA or MK801 to acutely block NMDA receptors revealed comparable recovery to nerves under control (ACSF) conditions. Similarly, NR1 mutant optic nerves had equivalent recoveries with or without D-AP5 treatment. Under Ca2+ free conditions control optic nerves recovered up to 98 ± 14 % (n = 8) whereas axons from NR1 mutants revealed a recovery of 65 ± 6 % (n = 7), $P < 0.05$ Student t test.
G, Wildtype optic nerves maintained *ex vivo* for 16 hours in oxygenated ACSF and treated with either NMDA/ Gly (100 μM), or NMDA/ Gly plus 7CKA/ D-AP5 (100 μM) or DMSO (solvent control), were tested for functional integrity and conductivity by applying increasing stimulus intensities (0 – 1 mA) in 0.1 mA steps. Depicted are stimulus-response relationships. Nerve conduction properties were tested at 2 and 16 hours of incubation for each treatment group. Note that there were no overt changes in nerve excitability over 16 hours of treatment, indicating functional integrity of optic nerves (See also Figure 4G).

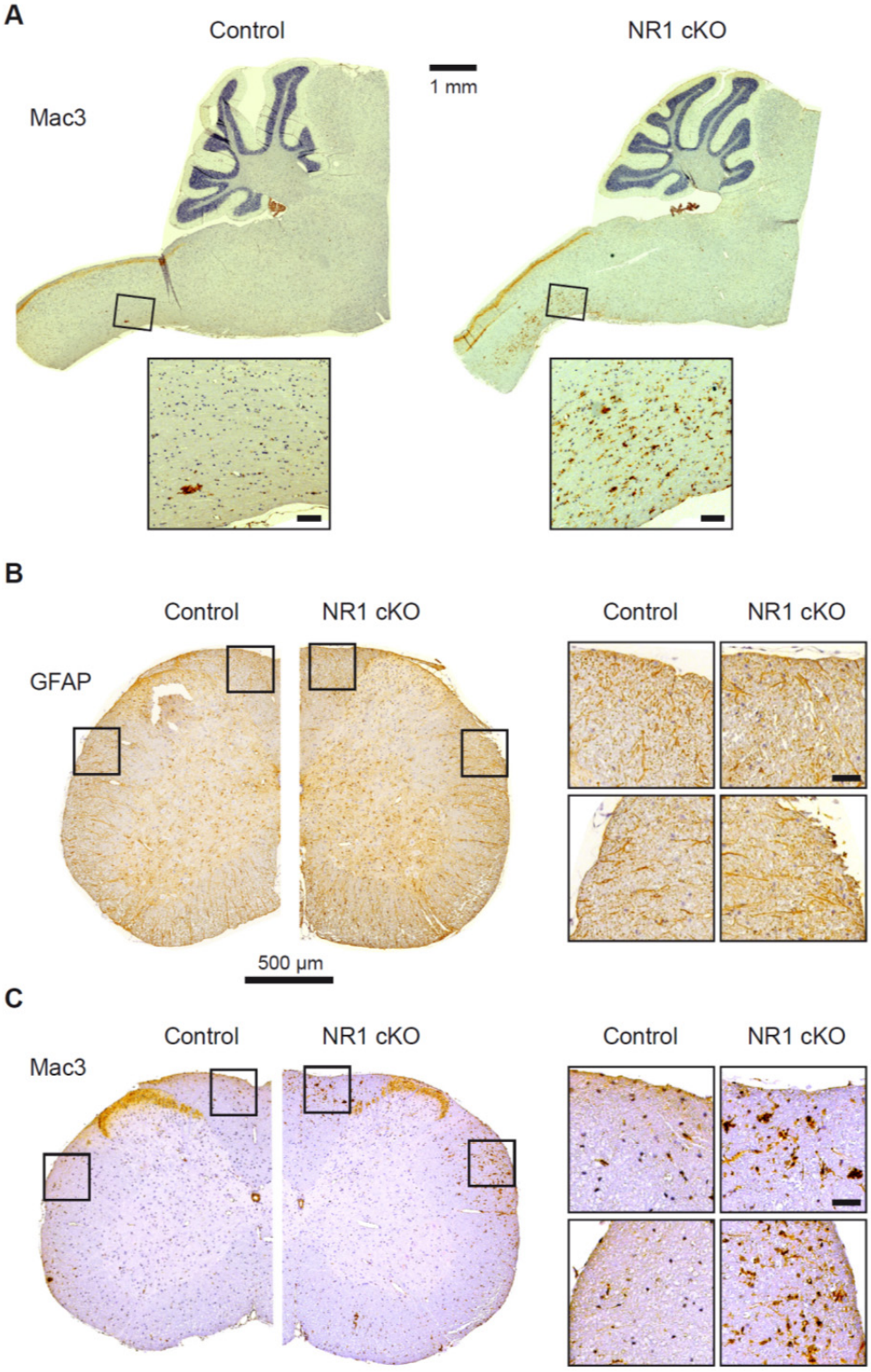

Figure S7 (Related to Figure 6). White matter tracts of brain stem and spinal cord show signs of inflammation
A, Depicted are longitudinal sections of cerebellum, brainstem and spinal cord (age 10 months), immunostained for activated microglia/macrophages (Mac3). In the ventral spinal cord, where the majority of cortico-spinal axons pass, we observed a significant increase of this inflammation marker in NR1 mutant mice (see also Figure 6).
B, **C** Spinal cord cross-sections from control and NR1 mutant mice stained (**B**) for astrogliosis (GFAP) and (**C**) for activated microglia/macrophages (Mac3).
Black boxes mark regions of higher magnifications; scale bars 100 µm (A) and 50 µm (B, C).

Supplemental Experimental Procedures

Purification of OPCs by immunopanning.

OPCs utilized for biotinylation assays, for measurements of 2-deoxyglucose uptake or lactate release by NMR were further purified to 98.2±0.3% by negative selection immunopanning (Barres et al., 1992). To selectively remove microglia, single cell suspensions of mechanically dissociated OPCs were incubated on Petri dishes coated with Bandeiraea simplicifolia (BS) lectin1(Cahoy et al., 2008) (2.3µg/ml, Vector labs) for 15 min at 37°C. To selectively remove astrocytes, unattached OPCs and astrocytes were then incubated for 30 min at 37°C on dishes sequentially coated with anti-mouse IgG antibody (Jackson Immunoresearch) and anti-rat neural antigen-2 (RAN-2) (Bartlett et al., 1981) antibody (i.e. conditioned media from RAN-2 hybridoma B lymphocytes (ATCC). The remaining purified OPCs were plated and differentiated as described in Experimental Procedures.

Glucose sensor FRET imaging

For glucose sensor confocal imaging, coverslips containing transfected primary oligodendrocytes were transferred to a custom made imaging chamber and continuously perfused with ACSF (in mM: NaCl 110.34; KCl 5.33; NaH_2PO_4 0.906; $NaHCO_3$ 44.05; $MgSO_4$ 0.814; $CaCl_2$ 1.8; glucose 10; adjusted to pH 7.4 with HCl after equilibration with 5% CO_2). The chamber was mounted on a Leica SP5 confocal microscope and cells were imaged using a HCX PL APO lambda blue 63x1.20 water-immersion objective. CFP was excited at 458 nm, and emission filters were set at 470-500 nm and 520-570 nm for detection of CFP and YFP fluorescence, respectively. Images were acquired every 10 s. Region of interests were set comprising the soma and the major processes of transfected oligodendrocytes. Background corrected mean fluorescence intensities were corrected for spectral bleed-through using correction factors obtained by transfecting primary oligodendrocytes with CFP or YFP only (Hou et al., 2011). Finally, corrected YFP fluorescence intensity obtained after excitation of CFP (= FRET) was divided by the corrected CFP fluorescence and the ratio (Fc/CFP) was normalized to the first 5 min of baseline recording, which was set as 1. NMDARs were activated by changing the perfusion solution to ACSF containing 100 µM NMDA and 100 µM glycine. Cells were preincubated with the antagonists of NMDA receptors (7CKA, 100 µM; D-AP5, 100 µM) for 30 min before NMDA and glycine were applied. For control experiments cells were incubated in ACSF lacking glucose or containing either iodoacetate (inhibitor of glycolysis, 1 mM) or cytochalasin B (inhibitor of glucose transpoter, 40 µM). From these data, the Fc/CFP signal was calibrated to cytosolic glucose concentrations using the k_D = 700 µM of the glucose sensor for glucose as described (Bittner et al., 2010). We have continuously monitored the cellular morphology of transfected oligodendrocytes by concomitant time lapse imaging to determine that drug applications (e.g. cytochalasin B) did not cause morphological changes that influence FRET signals.

NMR analysis

Conditioned media from untreated and 30 min NMDA/Gly (100 µM) treated immunopanned oligodendrocytes were snap frozen. Samples were mixed with 10% D_2O and the internal standard DSS and transferred to 3 mm NMR tubes. All spectra were recorded on an Avance Bruker 700 MHz spectrometer equipped with a cryogenic TXI $^{1}H/^{13}C$-$^{15}N/^{2}H$ probe head at 4°C. The ^{13}C, ^{1}H-HSQC experiments were done by acquisition of 2048 points in the direct dimension with spectral width of 13 ppm and 300 increments in the indirect dimension with spectral width of 95 ppm. The *J* coupling defocusing delay was set to 4 ms ($1/2^{1}J_{HC}$), the recycling time to 1.2 s and the total acquisition time was 3 hours and 46 minutes for each sample. A polynomial baseline correction was applied to the time domain signal. The latter was then zero filled to 4096 and 1024 points in the direct and indirect dimensions, respectively. Afterwards the time domain data were apodized by multiplication with a cosine function set to 0 at t_{1max} and Fourier transformed to the frequency domain in both dimensions. The data processing was performed using nmrPipe software (Delaglio et al., 1995). The integrations and quantifications were done using CARA (Keller, 2004).

Lactate release by fluorometric measurement of NADH

Lactate release from cultured oligodendrocytes was analysed as described for astrocytic cultures (Requardt et al., 2010). Mouse oligodendrocyte precursor cells were prepared as described above, 50,000 cells were seeded in wells of 24-well cell culture plates and were allowed to differentiate for 5 days in SATO medium. Cells were washed once with ACSF containing 10 mM glucose, and preincubated in 250 µl of ACSF (control) or ACSF containing 100 µM 7-CKA and/or 100 µM D-AP5 for 30 min. Then, cells were incubated in 250 µl ACSF with or without 100 µM NMDA and 100 µM glycine in the presence or absence of the inhibitors. For inhibition of glucose transporters, cytochalasin B was added in the concentrations indicated in the figures. After 15, 30 and 60 min of incubation 20 µl medium was removed and lactate content was determined using a reaction mixture consisting of 0.5 M glutamate buffer pH 8.9, 6 mM NAD^+, 35 µg/ml glutamate pyruvate transaminase and 50 µg/ml lactate dehydrogenase. After 60 min at 37 °C NADH fluorescence was determined using a plate reader and compared to wells containing known concentrations of lactate. Protein determination was done according to the Lowry method using bovine serum albumin as a standard.

Immunohistochemistry

Mice were anesthetized (2,2,2-tribromoethanol (2 % v/v) and amyl alcohol (2 % w/v, 0.2 ml/ 10 g body weight) and subsequently perfused with 4% paraformaldehyde (PFA) in 0.1 M sodium phosphate buffer. Brains and optic nerves were isolated and kept in the same fixative for 8-12 h at 4°C. After washing with PBS, optic nerves were cryoprotected with sucrose and frozen in OCT compound (Shandon Cryomatrix, Thermo Scientific) on dry ice. Nerve sections of 12 µm were made on a cryostat (Leica, Jung 2045C), mounted on superfrost slides (Superfrost Plus, Thermo Scientific) and air dried at room temperature (RT). Slide-mounted sections were washed with PBS and treated with 0.3% Triton X-100 and 5% horse serum for 1 h at RT. Brain sections of 40 µm were cut coronally with a vibratome (Leica, VT1000S) and treated similarly.

Primary antibodies were incubated over night at 4°C in 0.3% Triton X-100 and 5% horse serum. Dilutions were as follows: GFP (1:800, goat, Rockland; 1:500, rabbit, Abcam), CC1 (1:50, mouse, Calbiochem), Olig2 (1:200, rabbit, gift from C. D. Stiles, Boston, MA, USA), NG2 (1:200, rat, gift from J. Trotter, Mainz, Germany), GFAP (1:100, mouse, Novocastra), IBA1 (1:100, rabbit, Wako), NR1 (1:250, mouse, Zymed Laboratories), MBP (1:300, rabbit, Dako).

Secondary antibodies to mouse, rabbit and goat conjugated to Alexa 488-(1:2000 Molecular Probes), Alexa-555-(1:2000, Molecular Probes), Alexa-633(1:500, Molecular Probes), Cy2-(1:100, Dianova), Cy3-(1:1000, Dianova) and Cy5-(1:500, Dianova) were incubated in 2 % horse serum for 2 h at RT. For nuclei labeling DAPI (0.025 µg/ml final concentration) was added to the secondary antibody.

Confocal images were collected with a LSM 510 Meta microscope (Zeiss) using a 20x/0.5 Plan-Neofluar and 40x/1.2 water-immersion C-Apochromat objective. Excitation was performed at 488 nm, 543 nm and 633 nm, emission was detected for Alexa 488/Cy2, Alexa 555/Cy3 and Alexa 633/Cy5 at 500-530 nm band-pass, 560 nm long-pass and 650-710 nm band-pass filter sets, respectively. Z-stack images were taken at 0.5 – 1 µm intervals. For reporter analysis confocal stacks of 2-3 different sections from 3-4 individual animals were analyzed. For quantification of relative NR1 fluorescence intensities 9-12 confocal stacks of 3-4 different longitudinal optic nerve sections of 3 individual animals for each genotype were analyzed. The average fluorescence intensity for all stacks was calculated using ImageJ. Data were grouped per animal and normalized to controls.

Assessment of genomic recombination

Real time quantitative PCR (using SYBR Green and a 7500 Fast Real-Time PCR System, Applied Biosystems) was performed to amplify a DNA sequence of 184 bp flanking the 5' loxP site within the 5 kb intron between exons 10 and 11 of the floxed NR1 locus. Primers were located closely up- and downstream of the 5' loxP site and had the following sequence: sense 5'-GTCAAGCTTAGGATCCGGAACC-3' and anti-sense 5'-CAACTGCTCTTCCGAAGGTC-3'. Only non-recombined alleles would be amplified whereas after successful recombination the anti-sense primer could not anneal to its complementary strand impeding the PCR amplification. Genomic DNA was isolated from optic nerves of individual animals. For each sample four technical replicates per PCR were implemented. Neuregulin 1 type III (NrgIII) (sense 5'-GTGTGCGGAGA-AGGAGAAAACT-3' and anti-sense 5'-AGGCACAGAGAGGAATTCATTTCTTA-3') and Gria1 (sense 5'-CCAGGTGTCTT-CTCCTTTCTTG-3' and anti-sense 5'-CTGAAACGGCTGACCAGG-3') were used as endogenous gene controls. Data normalization and analysis were performed with the 7500 Fast System Software. This approach enabled a relative quantification of the extent of recombined alleles in the optic nerves of NR1 cKO mice.

Electron microscopy

Following tissue preparation and fixation, samples were dehydrated in a graded series of ethanol, and then embedded in Epon. For HPF freshly dissected optic nerves were placed in an aluminum specimen carrier with a 0.1 mm or 0.2 mm indentation (Microscopy Services, Kiel, Germany). Remaining space was covered with yeast paste or 20% PVP in PBS, and the sample was cryofixed in a Bal-Tec HPM010 high-pressure freezer (former Bal-Tec, now ABRA-Fluid AG, Widnau, Switzerland). Freeze-substitution was carried out in a Leica AFS (Leica, Vienna, Austria) as follows: Samples were first kept in tannic acid (Sigma-Aldrich) 0.1% in acetone at −90°C for 100 h, washed with acetone (4 x 30 min, −90°C), and then transferred into OsO_4 (Science Services, Munich, Germany) 2 % in acetone, −90°C. The temperature was raised from −90°C to −20°C in increments of 5°C/h, then kept unaltered at −20°C for 16 h, and then raised from −20°C to +4°C in increments of 10°C/h. Then the samples were washed with acetone (3 x 60 min at 4°C), allowed to adjust to room temperature (1 h), and finally transferred into Epon (Serva) (50% Epon in acetone for 3 h, 90% Epon in acetone for 18 h, 100% Epon for 6 h). The samples were placed in an embedding mold and polymerized (60°C, 24 h). Ultrathin sections (50 nm) were cut using a Leica Ultracut S ultramicrotome (Leica, Vienna, Austria) and stained with an aqueous solution of 2% uranyl acetate (Merck, Darmstadt, Germany) followed by lead citrate (Reynolds, 1963).

Optic nerve recordings analysis

Acutely isolated optic nerves were stimulated and recorded from by custom-made suction electrodes back-filled with ACSF [(in mM): 124 NaCl, 3.0 KCl, 2.0 $CaCl_2$, 2.0 $MgSO_4$, 1.25 NaH_2PO_4, 23 $NaHCO_3$, and 10 glucose]. The stimulation electrode was connected to a stimulus isolator (385, WPI) to evoke compound action potentials (CAP). The recording electrode was connected to a Heka amplifier (EPC9), and the signal was amplified 500 times, filtered at 30 kHz, and acquired at 20-30 kHz. Before recording, optic nerves were equilibrated for at least 15 min in the chamber. Square-wave constant current stimulus

pulse (50 µs) strength was adjusted to evoke the maximum CAP possible, and then increased an additional 25 % for supramaximal stimulation.

Stimulus-response relationships were performed by varying stimulus intensity from 0.1 to 1 mA and measuring the area of the corresponding graded CAPs. This protocol allowed for comparison of the relative thresholds of activation of the population of conducting fibers. The CAP area was expressed as percentage of the last CAP area (at maximum stimulation of 1 mA) in the train.

The CAP latency was measured (at supramaximal stimulation after averaging 50 CAPs elicited every 30 s) as the time between the onset of the stimulus artefact to the first, second and third peak as previously described (Baltan et al., 2010). The suction electrode recording configuration at supramaximal stimulation allows all axons in optic nerves to be activated and the resultant action potential from each axon to be recorded. This method has the advantage of enabling stable recording of three-peaked characteristic shape of CAPs. These peaks reflect three sub-groups of axon populations based on their conduction velocity and the area under the CAP reflecting the number of contributing axons (Cummins et al., 1979).

For pharmacology of OGD recordings the following experiments were performed. A Ca^{2+}-free ACSF was used in some experiments and contained 200 µM EGTA and 4 mM Mg^{2+} (to maintain constant divalent cation concentration). Control experiments indicated that CAPs remained essentially unchanged in this solution (with normal glucose and oxygen) for at least 90 min. 7-chlorokynurenic acid (7-CKA, 50 µM; dissolved in DMSO as 50 mM stock), D-(-)-2-Amino-5-phosphonopentanoic acid (D-AP5, 100 µM) and MK801 (50 µM, dissolved in DMSO as 50 mM stock) were used to block NMDA receptors during recordings. Optic nerves treated with pharmacological substances or Ca^{2+}-free ACSF were incubated 30 min before, during and 30 min after OGD.

Surgery for in vivo spinal cord CAP recordings

Surgery for in vivo spinal cord recordings was slightly modified as previously described (Dibaj et al., 2012; Steffens et al., 2012). Anaesthesia was initiated by 80 mg/kg pentobarbital injected i. p. After cannulation of the jugular vein, anesthesia was continued with 40-60 mg methohexital per kg and h. A tracheotomy was performed and a tube inserted for artificial ventilation. Active respiratory movements were abolished by paralysis with pancuronium (800 µg per kg supplemented i.p. every hour) and artificial ventilation with a gas mixture of CO_2 (2.5 %), O_2 (47.5 %), and N_2 (50 %) at 120 strokes/min (100-160 µl/stroke depending on the body weight) was performed. Body temperature, heart rate and O_2 blood saturation were continuously monitored and also used to control the level of anesthesia. The vertebral column was rigidly fixed with two custom-made clamps. A laminectomy was performed from vertebrae TH13 to L5 to expose the spinal cord segments L1 to L4 as well as to expose the dorsal roots L3 to L5. For electrophysiology, the spinal cord was covered with mineral oil.

Behavioural assessment of visual acuity and contrast sensitivity

Visual acuity and contrast sensitivity response were assessed using the virtual-reality optomotor system (Douglas et al., 2005; Prusky et al., 2004). In the optomotor system freely moving animals were exposed to moving sine wave gratings of various spatial frequencies, contrasts and drift speeds and reflexively tracked this pattern by head movements as long as they could see it. Experimenters were blind to the animal's genotype and thresholds were regularly validated independently by more than one observer.

Experimental autoimmune encephalomyelitis (EAE) induction

EAE experiments were carried out in 8-12 week-old mice as described earlier (Matute et al., 2007). Briefly, chronic, relapsing EAE was induced in littermate control and in NR1 cKO mice, by immunization with 300 µl of myelin oligodendrocytes glycoprotein 35–55 [MOG(35–55)] (200 µg; Sigma) in incomplete Freund's adjuvant supplemented with 8 mg/ml *Mycobacterium tuberculosis* H37Ra. Pertussis toxin (500 ng; Sigma) was injected intraperitoneally on the day of immunization and again 2 d later. In all instances, motor symptoms were recorded daily and scored as follows from 0 to 8: 0, no detectable changes in muscle tone and motor behaviour; 1, flaccid tail; 2, paralyzed tail; 3, impairment or loss of muscle tone in hind limbs; 4, hind limb hemi-paralysis; 5, complete hind limb paralysis; 6, complete hind limb paralysis and loss of muscle tone in forelimbs; 7, tetraplegia; and 8, moribund. Conduction velocity of the corticospinal tract was assessed in anesthetized mice with tribromoethanol (240 mg/kg, i.p.; Sigma) using stimulatory and recording electrodes placed in the primary motor cortex and in the vertebral canal at the L2 level, respectively. After recording, mice were fixed, and spinal cord was processed for immunohistochemistry. Tissue blocks of spinal cords were cryoprotected, cut longitudinally (10 µm thick), and stained with toluidine blue and antibody to CC1 (1 µg/ml; Calbiochem, Barcelona, Spain).

Supplemental References

Baltan, S., Inman, D.M., Danilov, C.A., Morrison, R.S., Calkins, D.J., and Horner, P.J. (2010). Metabolic vulnerability disposes retinal ganglion cell axons to dysfunction in a model of glaucomatous degeneration. JNeurosci *30*, 5644-5652.

Barres, B.A., Hart, I.K., Coles, H.S., Burne, J.F., Voyvodic, J.T., Richardson, W.D., and Raff, M.C. (1992). Cell death and control of cell survival in the oligodendrocyte lineage. Cell *70*, 31-46.

Bartlett, P.F., Noble, M.D., Pruss, R.M., Raff, M.C., Rattray, S., and Williams, C.A. (1981). Rat neural antigen-2 (RAN-2): a cell surface antigen on astrocytes, ependymal cells, Muller cells and lepto-meninges defined by a monoclonal antibody. Brain research *204*, 339-351.

Bittner, C.X., Loaiza, A., Ruminot, I., Larenas, V., Sotelo-Hitschfeld, T., Gutierrez, R., Cordova, A., Valdebenito, R., Frommer, W.B., and Barros, L.F. (2010). High resolution measurement of the glycolytic rate. Frontiers in neuroenergetics *2*.

Cahoy, J.D., Emery, B., Kaushal, A., Foo, L.C., Zamanian, J.L., Christopherson, K.S., Xing, Y., Lubischer, J.L., Krieg, P.A., Krupenko, S.A.*, et al.* (2008). A transcriptome database for astrocytes, neurons, and oligodendrocytes: a new resource for understanding brain development and function. JNeurosci *28*, 264-278.

Cummins, K.L., Dorfman, L.J., and Perkel, D.H. (1979). Nerve fiber conduction-velocity distributions. II. Estimation based on two compound action potentials. ElectroencephalogrClinNeurophysiol *46*, 647-658.

Delaglio, F., Grzesiek, S., Vuister, G.W., Zhu, G., Pfeifer, J., and Bax, A. (1995). NMRPipe: a multidimensional spectral processing system based on UNIX pipes. Journal of biomolecular NMR *6*, 277-293.

Dibaj, P., Zschuntzsch, J., Steffens, H., Scheffel, J., Goricke, B., Weishaupt, J.H., Le Meur, K., Kirchhoff, F., Hanisch, U.K., Schomburg, E.D.*, et al.* (2012). Influence of methylene blue on microglia-induced inflammation and motor neuron degeneration in the SOD1(G93A) model for ALS. PloS one *7*, e43963.

Douglas, R.M., Alam, N.M., Silver, B.D., McGill, T.J., Tschetter, W.W., and Prusky, G.T. (2005). Independent visual threshold measurements in the two eyes of freely moving rats and mice using a virtual-reality optokinetic system. VisNeurosci *22*, 677-684.

Hou, B.H., Takanaga, H., Grossmann, G., Chen, L.Q., Qu, X.Q., Jones, A.M., Lalonde, S., Schweissgut, O., Wiechert, W., and Frommer, W.B. (2011). Optical sensors for monitoring dynamic changes of intracellular metabolite levels in mammalian cells. NatProtoc *6*, 1818-1833.

Keller, R. (2004). Computer Aided Resonance Assignment. http://cara.nmr.ch.

Matute, C., Torre, I., Perez-Cerda, F., Perez-Samartin, A., Alberdi, E., Etxebarria, E., Arranz, A.M., Ravid, R., Rodriguez-Antiguedad, A., Sanchez-Gomez, M.*, et al.* (2007). P2X(7) receptor blockade prevents ATP excitotoxicity in oligodendrocytes and ameliorates experimental autoimmune encephalomyelitis. JNeurosci *27*, 9525-9533.

Prusky, G.T., Alam, N.M., Beekman, S., and Douglas, R.M. (2004). Rapid quantification of adult and developing mouse spatial vision using a virtual optomotor system. Invest OphthalmolVisSci *45*, 4611-4616.

Requardt, R.P., Wilhelm, F., Rillich, J., Winkler, U., and Hirrlinger, J. (2010). The biphasic NAD(P)H fluorescence response of astrocytes to dopamine reflects the metabolic actions of oxidative phosphorylation and glycolysis. Journal of neurochemistry *115*, 483-492.

Reynolds, E.S. (1963). The use of lead citrate at high pH as an electron-opaque stain in electron microscopy. JCell Biol *17*, 208-212.

Steffens, H., Dibaj, P., and Schomburg, E.D. (2012). In vivo measurement of conduction velocities in afferent and efferent nerve fibre groups in mice. Physiol Res *61*, 203-214.